Inorganic Chemistry
Article

Inorg. Chem. **2009**, *48*, 5187–5194 **5187**
DOI: 10.1021/ic9000973

Spectroscopy and Electronic Structures of $Ru_2(ap)_4$-alkynyl Compounds

Lei Zhang,[†] Bin Xi,[†] Isiah Po-Chun Liu,[†] M. M. R. Choudhuri,[‡] Robert J. Crutchley,[‡] James B. Updegraff,[§] John D. Protasiewicz,[§] and Tong Ren*[,†]

[†]*Department of Chemistry, Purdue University, 560 Oval Drive, West Lafayette, Indiana 47907,* [‡]*Department of Chemistry, Carleton University, Ottawa, Ontario K1S 5B6, Canada, and* [§]*Department of Chemistry, Case Western Reserve University, Cleveland, Ohio 44106*

Received January 19, 2009

A new N,N′-bidentate ligand, 2-(3-isobutoxyanilino)pyridine (H^{t}BuOap), was introduced and used as the ancillary ligand to support highly soluble diruthenium compounds. Thus, the new compounds $Ru_2(^t$BuOap$)_4$Cl (**1**), $Ru_2(^t$BuOap$)_4$(C≡CPh) (**2**), $Ru_2(^t$BuOap$)_4$(C≡CPh)$_2$ (**3**), and $Ru_2(^t$BuOap$)_4$(C≡CSi^{i}Pr$_3$) (**4**) were prepared and characterized by both voltammetric and spectroscopic methods, and their physical properties were found to be quite similar to those of the previously reported $Ru_2(ap)_4$-based compounds. The spectroscopic properties of both anionic and cationic derivatives of compounds **2** and **3** were examined with spectroelectrochemistry. Density functional theory calculations performed on model compounds of **2** and **3** provide an in-depth picture of the electronic structures of $Ru_2(ap)_4$-based alkynyl compounds and assignment of the observed electronic transitions.

Introduction

Metal-alkynyl species have received intense interest as materials for electronic and optoelectronic applications.[1−7] Our interest in this area focuses on the utility of diruthenium alkynyls as active materials for molecular devices,[8,9] and both the wire-like behavior and conductance switching have been demonstrated with the mono- and bis-alkynyl derivative of $Ru_2(ap)_4$ (ap = 2-anilinopyridinate), respectively.[10,11] Among hundreds of diruthenium alkynyl species known to date,[8,12] $Ru_2(ap)_4$(C≡CPh) reported by Chakravarty and Cotton holds a special place, being the first example of bimetallic species containing a σ-acetylide ligand.[13] Kadish, Bear, and co-workers reported many alkynyl species based on $Ru_2(ap)_4$, $Ru_2(F_xap)_4$ ($F_x$ap is a perfluorinated or partially fluorinated ap ligand), and $Rh_2(ap)_4$,[14−18] where the coexistence of regio-isomers due to the orientation of $F_x$ap ligands is noteworthy. Building on Cotton's pioneering work, our laboratory further elucidated the formation of related mono-alkynyl species[19−21] and uncovered the bis-alkynyl $Ru_2(ap)_4$ derivatives.[22−24] The successful preparation of polyyn-diyls capped by $Ru_2(ap)_4$ termini, namely, $[Ru_2(ap)_4]_2(\mu$-$C_{2n})$ with n = 1−4 and 6, enables us to probe the charge-transfer processes across polyyn-diyl chains.[25−27] Despite these successes, synthetic and subsequent characterization efforts are

*To whom correspondence should be addressed. E-mail: tren@purdue.edu.

(1) Paul, F.; Lapinte, C. *Coord. Chem. Rev.* **1998**, *178−180*, 431.
(2) Low, P. J. *Dalton Trans.* **2005**, 2821.
(3) Wong, W.-Y.; Ho, C.-L. *Coord. Chem. Rev.* **2006**, *250*, 2627.
(4) Whittall, I. R.; McDonagh, A. M.; Humphrey, M. G.; Samoc, M. *Adv. Organomet. Chem.* **1999**, *43*, 349.
(5) Bruce, M. I.; Low, P. J. *Adv. Organomet. Chem.* **2004**, *50*, 179.
(6) Paul, F.; Lapinte, C. In *Unusual structures and physical properties in organometallic chemistry*; Gielen, M., Willem, R., Wrackmeyer, B., Eds.; Wiley: West Sussex, U.K., 2002.
(7) Yam, V. W.-W. *Acc. Chem. Res.* **2002**, *35*, 555.
(8) Ren, T. *Organometallics* **2005**, *24*, 4854.
(9) Xi, B.; Ren, T. *C. R. Chimie* **2009**, *12*, 321.
(10) Blum, A. S.; Ren, T.; Parish, D. A.; Trammell, S. A.; Moore, M. H.; Kushmerick, J. G.; Xu, G.-L.; Deschamps, J. R.; Pollack, S. K.; Shashidhar, R. *J. Am. Chem. Soc.* **2005**, *127*, 10010.
(11) Mahapatro, A. K.; Ying, J.; Ren, T.; Janes, D. B. *Nano Lett.* **2008**, *8*, 2131.
(12) Angaridis, P. In *Multiple Bonds between Metal Atoms*; Cotton, F. A., Murillo, C. A., Walton, R. A., Eds.; Springer Science and Business Media, Inc.: New York, 2005.
(13) Chakravarty, A. R.; Cotton, F. A. *Inorg. Chim. Acta* **1986**, *113*, 19.
(14) Bear, J. L.; Li, Y.; Han, B.; Caemelbecke, E. V.; Kadish, K. M. *Inorg. Chem.* **1997**, *36*, 5449.
(15) Bear, J. L.; Han, B.; Wu, Z.; Caemelbecke, E. V.; Kadish, K. M. *Inorg. Chem.* **2001**, *40*, 2275.
(16) Kadish, K. M.; Phan, T. D.; Giribabu, L.; Caemelbecke, E. V.; Bear, J. L. *Inorg. Chem.* **2003**, *42*, 8663.
(17) Kadish, K. M.; Phan, T. D.; Wang, L.-L.; Giribabu, L.; Thuriere, A.; Wellhoff, J.; Huang, S.; Caemelbecke, E. V.; Bear, J. L. *Inorg. Chem.* **2004**, *43*, 4825.
(18) Nguyen, M.; Phan, T.; Caemelbecke, E. V.; Kajonkijya, W.; Bear, J. L.; Kadish, K. M. *Inorg. Chem.* **2008**, *47*, 7775.
(19) Zou, G.; Alvarez, J. C.; Ren, T. *J. Organomet. Chem.* **2000**, *596*, 152.
(20) Hurst, S. K.; Ren, T. *J. Organomet. Chem.* **2002**, *660*, 1.
(21) Xi, B.; Xu, G.-L.; Ying, J.-W.; Han, H.-L.; Cordova, A.; Ren, T. *J. Organomet. Chem.* **2008**, *693*, 1656.
(22) Xu, G.-L.; Ren, T. *Organometallics* **2001**, *20*, 2400.
(23) Xu, G.-L.; Ren, T. *J. Organomet. Chem.* **2002**, *655*, 239.
(24) Ren, T. *Organometallics* **2002**, *21*, 732.
(25) Ren, T.; Zou, G.; Alvarez, J. C. *Chem. Commun.* **2000**, 1197.
(26) Xu, G.-L.; Zou, G.; Ni, Y.-H.; DeRosa, M. C.; Crutchley, R. J.; Ren, T. *J. Am. Chem. Soc.* **2003**, *125*, 10057.
(27) Shi, Y.; Yee, G. T.; Wang, G.; Ren, T. *J. Am. Chem. Soc.* **2004**, *126*, 10552.

Published on Web 05/01/2009

Scheme 1. $Ru_2(^i BuOap)_4$-Based Compounds **1**−**4** and Related Hap Ligands

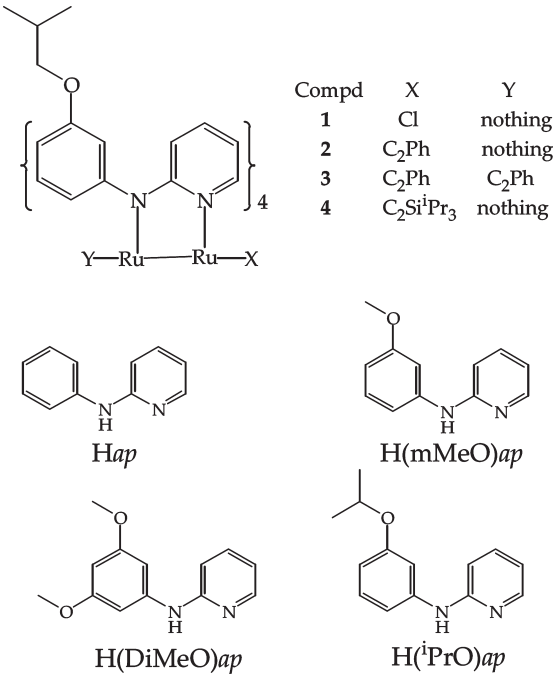

often hindered by the poor solubility of $Ru_2(ap)_4$-based compounds, causing us to introduce several aniline-substituted derivatives, Xap, as shown in Scheme 1. Previous studies of modified ap ligands include those based on *m*-MeOap, *m*-^{i}PrOap, or DiMeOap, and the resultant diruthenium species exhibited varying degrees of improvement in organic solubility.[21,28] As described in this contribution, the introduction of a *m*-^{i}BuO substituent results in such a pronounced enhancement of the solubility that $Ru_2(^i BuOap)_4Cl$ is even slightly soluble in hexanes.

In addition to solving the issues of organic solubility, there also remain unresolved and yet important issues concerning the electronic structures of $Ru_2(ap)_4$-type compounds. For instance, it has been established experimentally that the mono-alkynyl species are of an $S = {}^3/_2$ ground state, while the bis-alkynyl species are diamagnetic ($S = 0$). Yet, an in-depth theoretical analysis of electronic structures is absent, which significantly limits the ability to discern the orbital origins of the observed optical transitions and redox couples. Furthermore, the interesting current−voltage characteristics measured at the single-molecule level are intimately related to the *change* in electronic structures upon injection of an electron (reduction) or a hole (oxidation).[10,11] A two-prong approach was adopted to address these issues: high-level density functional theory (DFT) calculations (*ADF*[29] and *Gaussian 03*[30]) were employed to elucidate the electronic structures of both the neutral and charged $Ru_2(ap)_4$ species, and changes in electronic structures upon oxidation/reduction are experimentally probed using spectroelectrochemistry.

(28) Xu, G.-L.; Cordova, A.; Ren, T. *J. Cluster Sci.* **2004**, *15*, 413.
(29) *ADF2006.01 SCM*; Theoretical Chemistry, Vrije Universiteit: Amsterdam, The Netherlands, 2006.
(30) Frisch, M. J.; et al. *Gaussian 03*, revision D.02; Gaussian, Inc.: Wallingford, CT, 2003.

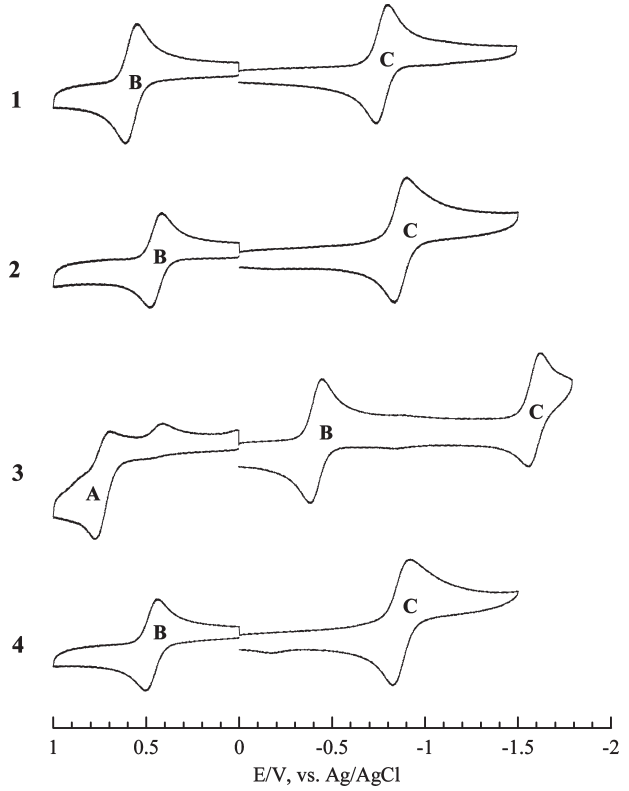

Figure 1. Cyclic voltammograms of compounds **1**−**4** recorded in a 0.20 M THF solution of Bu_4NPF_6 at a scan rate of 100 mV/s.

Results and Discussion

Synthesis. The ligand H^{i}BuOap was prepared from the reaction between 3-isobutoxyphenylamine and 2-bromopyridine and characterized by both ^{1}H NMR spectroscopic and single-crystal X-ray diffraction studies. Compound $Ru_2(^i BuOap)_4Cl$ (**1**) was prepared from refluxing a mixture of $Ru_2(OAc)_4Cl$ and H ^{i}BuOap in toluene using the setup described for $Ru_2(ap)_4Cl$.[19] A prolonged reaction time was necessary to ensure a high yield of the (4,0) isomer (see the Experimental Section). Compounds $Ru_2(^i BuOap)_4(C{\equiv}CPh)$ (**2**) and $Ru_2(^i BuOap)_4(C{\equiv}CSi^i Pr_3)$ (**4**) were prepared from the reaction between $Ru_2(^i BuOap)_4Cl$ and 1 equiv of LiC≡CR (R = Ph and $Si^i Pr_3$), while $Ru_2(^i BuOap)_4(C{\equiv}CPh)_2$ (**3**) was prepared from the reaction between **1** and three equiv of LiC≡CPh. Compounds **1**−**4** are highly soluble in polar organic solvents, such as tetrahydrofuran (THF) and CH_2Cl_2, and slightly soluble in hexanes. While the free ligand H^{i}BuOap was crystallized and characterized by X-ray diffraction (see Figure 9 in the Experimental Section), attempts to obtain single crystals of compounds **1**−**4** all failed, indicating the diminishing crystallinity with a much improved solubility. Compounds **1**, **2**, and **4** are paramagnetic with effective moments ranging from 3.60 to 3.97 μ_B, which is consistent with an $S = {}^3/_2$ ground state. Although not characterized by ^{1}H NMR, these paramagnetic species were analyzed satisfactorily by combustion analysis. Similar to other previously reported $Ru_2(ap)_4(C{\equiv}CR)_2$ compounds, compound **3** is diamagnetic and displays a well-resolved ^{1}H NMR spectrum.

Electrochemistry. Cyclic voltammograms of compounds **1**−**4** were measured in THF and are shown in Figure 1. The mono-axially ligated species **1**, **2**, and **4**

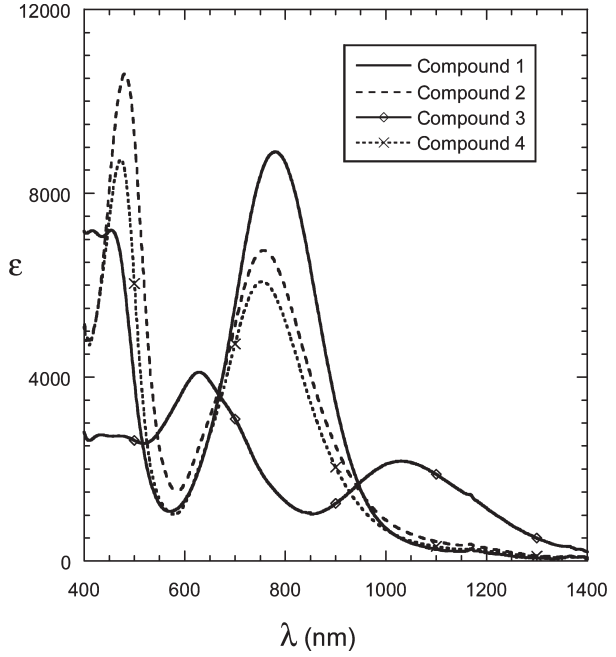

Figure 2. Visible−NIR absorption spectra of compounds **1**−**4** recorded in THF.

Scheme 2. Assignments of the Observed Redox Couples

$$Ru_2(III,IV) \underset{A}{\overset{-e^-}{\longleftarrow}} Ru_2(III,III) \underset{B}{\overset{+e^-}{\rightleftharpoons}} Ru_2(III,II) \underset{C}{\overset{+e^-}{\rightleftharpoons}} Ru_2(II,II)$$

exhibit two one-electron processes: an oxidation (B) and a reduction (C). The bisphenylacetylide compound **3** undergoes an irreversible one-electron oxidation (A) and two one-electron reductions (B and C). As indicated in Scheme 2, all three observed redox couples are Ru_2-based, which is consistent with prior studies of $Ru_2(ap)_4$ species.[13,19,21,23,24,28] It is noteworthy that the electrode potentials ($E_{1/2}$) for the same couple are almost identical within experimental error among Ru_2 compounds supported by ap and its aniline-substituted surrogates mentioned in Scheme 1. For instance, the first reduction (B) of bisphenylacetylide compounds occurs at −0.415 V for compound **3** and −0.418 V for the compound based on ap.[23] The excellent agreement reflects a minimal alteration in electronic structures due to the introduction of alkoxy substituents at the aniline ring.

Visible−Near-IR (NIR) Spectroscopy. As shown in Figure 2, compound **1** absorbs intensely at 780 and 420−460 nm, while the mono-alkynyl species **2** and **4** have a slightly less intense band at ca. 755 nm and a more intense band at ca. 477 nm. The spectrum of compound **3**, the only bis-alkynyl species, features two broad absorptions centered at 1030 and 630 nm and two minor peaks at 469 and 433 nm. These results are in accordance with the prior reports of $Ru_2(ap)_4$-based compounds,[13,19,21,23,24,26,28] and assignments of the observed transitions are given below.

DFT Calculations. The nature of electronic structures of Ru_2^{n+} (n = 5 and 6) species has always been an interesting challenge. Because of the near-degeneracy of the π^*(Ru−Ru) and δ^*(Ru−Ru) orbitals, the Ru_2^{5+} species may have a ground state of either $S = {}^3/_2$ or ${}^1/_2$,[31,32] while the Ru_2^{6+} species has a ground state of S = 2, 1, or 0.[33] The ground-state configuration of a diruthenium species can be unambiguously assigned based on the temperature dependence of magnetic susceptibility and interpreted using phenomenological (ligand-field-type) models.[32] However, such analyses do not yield quantitative information about the energies of frontier orbitals and hence cannot provide insights on electronic spectra. To overcome these problems, DFT calculations were performed on the model compounds of $Ru_2(ap)_4L_x$ (x = 1 and 2), **Model1** and **Model2**, where the phenyl ring of the ap ligand was replaced by a methyl group and acetylide was used as the axial ligand(s) (Scheme 3).

Table 1. Relevant Geometrical Parameters (Å) and Results Optimized for **Model1**

	$\sigma^2\pi^4\delta^2\pi^{*2}\delta^{*1}$			$\sigma^2\pi^4\delta^2\pi^{*3}$	$\sigma^2\pi^4\delta^2\pi^{*1}\delta^{*2}$	
	GBI	GBII	ABI	ABI	ABI	exp[b]
Ru1−Ru2	2.355	2.349	2.352	2.434	2.306	2.33
Ru1−N_{ap}	2.062	2.074	2.059	2.023	2.083	2.047
Ru2−N_p	2.142	2.159	2.134	2.100	2.156	2.108
Ru2−C	2.073	2.077	2.064	2.041	2.052	2.075
Spin Distribution [a]						
Ru1	1.78	1.76	1.59	0.57	0.72	
Ru2	0.84	0.83	0.90	0.43	0.47	
$\triangle E$ (eV)			0	0.049	1.287	

[a] Spin distribution (number of electrons spin-α minus spin-β). [b] Average of the observed values.[8]

Scheme 3. Model Compounds Used in DFT Calculations

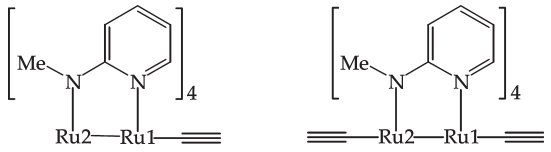

Model1 Model2

Listed in Table 1 are the results of the geometry optimizations of **Model1** by different functionals and basis sets. The ground-state electronic configuration of **Model1** is $\sigma^2\pi^4\delta^2\pi^{*2}\delta^{*1}$ (Figure 3), which is consistent with the $S = {}^3/_2$ ground state determined for $Ru_2(ap)_4C_2R$.[8,34] The relative energies of excited-state configurations with respect to the $\sigma^2\pi^4\delta^2\pi^{*2}\delta^{*1}$ configuration are +0.049 eV for $\sigma^2\pi^4\delta^2\pi^{*3}$ ($S = {}^1/_2$) and +1.287 eV for $\sigma^2\pi^4\delta^2\pi^{*1}\delta^{*2}$ ($S = {}^1/_2$). In addition to the minimal energy, the calculated bond distances of the $\sigma^2\pi^4\delta^2\pi^{*2}\delta^{*1}$ configuration are in good agreement with those determined by single-crystal X-ray diffraction studies ($Ru_2(ap)_4$-based compounds).[8] The spin distribution indicates that Ru1 and Ru2 may be assigned to Ru^{2+} (1.78, two unpaired electrons) and Ru^{3+}

(31) Norman, J. J. G.; Renzoni, G.; Case, D. A. *J. Am. Chem. Soc.* **1979**, *101*, 5256.

(32) Miskowski, V. M.; Hopkins, M. D.; Winkler, J. R.; Gray, H. B. In *Inorganic Electronic Structure and Spectroscopy*; Solomon, E. I., Lever, A. B. P., Eds.; Wiley: New York, 1999.

(33) Cotton, F. A.; Yokochi, A. *Inorg. Chem.* **1997**, *36*, 567.

(34) Ren, T.; Xu, G.-L. *Comments Inorg. Chem.* **2002**, *23*, 355.

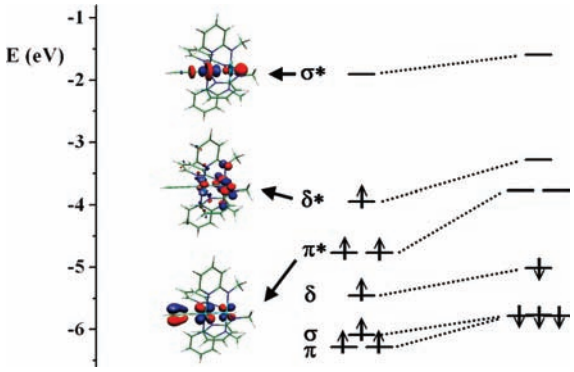

Figure 3. Molecular orbital diagram for **Model1** obtained from DFT calculations (ABI). The α and β counterparts of molecular orbitals are connected with the broken lines.

Table 2. Relevant Geometrical Parameters (Å) and Results Computed for **Model2**

	GBI[a]	GBII[a]	GBI(FZ)[a,b]	ABI[a]	ABII[a]	ABI(BS)[c]	exp[d]
Ru1−Ru2	2.632	2.619	2.470	2.602	2.592	2.534	2.47
Ru1−N_{ap}	2.054	2.067	2.051	2.048	2.050	2.057[d]	2.031
Ru2−N_p	2.096	2.115	2.092	2.081	2.083	2.089[d]	2.042
Ru_1−C	1.947	1.950	1.946	1.934	1.939	2.041	1.959
Ru_2−C	1.939	1.941	1.938	1.922	1.923	2.018	1.938
ΔE (eV)				0		0.256	

[a] Electronic configuration ($\pi^4\delta^2\pi^{*4}$). [b] Fixed Ru−Ru distance (2.47 Å). [c] Broken-symmetry electronic configuration ($\pi^4\delta^2\pi^{*3}\sigma^1$) as described in the text. [d] Average of the X-ray structural data.[8]

(0.84, one unpaired electron), respectively. Because of the strong Ru−Ru bonding (1 σ, 1 π, and 0.5 δ), the three unpaired electrons are delocalized between two Ru centers.

For **Model2**, most of the optimized bond distances around the Ru_2^{6+} core agree well with those determined from X-ray studies (Table 2) with the exception of the Ru−Ru bond length, which is about 0.15 Å longer than the experimental value. A similar discrepancy between the calculated and measured Ru−Ru bond lengths was noted in an early study of $Ru_2^{III,III}$ species[35] and may be attributed to the underestimation of metal−metal interaction by both the DFT method[36−39] and the utilization of an effective core potential in the atomic basis sets.[40] Several different functionals and basis sets were invoked to improve the optimized Ru−Ru distance (Table 2), but the result is independent of the method used. The calculated Ru−Ru bond length from the ABII method is the closest to the experimental value but still overestimated.

The calculated electronic configuration of **Model2** is $\pi^4\delta^2\pi^{*4}$ (Figure 4), which is in accordance with the

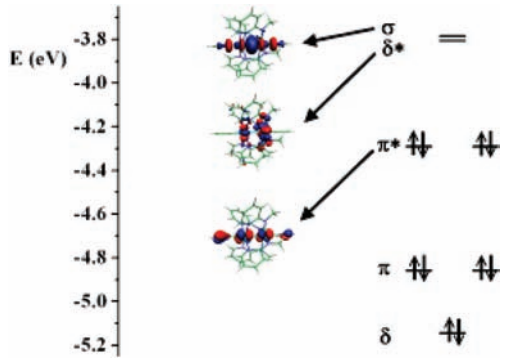

Figure 4. Molecular orbital diagram for **Model2** obtained from DFT calculations (ABI).

original proposal by Bear et al.[41] and Cotton and Yokochi.[33] In order to explore other configurations that may lead to a Ru−Ru distance matching the measured value, one β-spin electron was moved from the π^*(Ru−Ru) orbital to an unoccupied σ-type orbital of some Ru−Ru bonding character. The resulting broken-symmetry configuration ($\pi^4\delta^2\pi^{*3}\sigma^1$) does have a shorter Ru−Ru distance [Table 2, ABI(BS)]. However, the addition of a β-spin electron in the σ orbital lengthens the Ru−C bond by ca. 0.08 Å because of the Ru−C antibonding character in this orbital. In addition, the energy of this state is 0.256 eV higher than that of the $\pi^4\delta^2\pi^{*4}$ configuration, suggesting that the $\pi^4\delta^2\pi^{*3}\sigma^1$ configuration is not a reasonable ground state. ADF calculation with the $\pi^4\delta^2\pi^{*2}\delta^{*2}$ configuration ($S = 0$) was also attempted but failed to converge, which is likely due to the nonaufbau nature of the configuration.

To further explore the relationship between the electronic configuration and Ru−Ru bond length, the Ru−Ru distance was fixed at the observed value of 2.47 Å and the rest of the structure was optimized. The calculation [GBI(FZ)] yielded the same $\pi^4\delta^2\pi^{*4}$ ground-state configuration as that for **Model2**. It has been established *experimentally* that Ru_2^{6+} species of the same electronic configuration $\pi^4\delta^2\pi^{*4}$ display a broad range of Ru−Ru distances (2.44−2.56 Å).[33,35,41−43] The significant variation reflects the weak nature of the δ bond and a stronger dependence on the bridging ligand. The simplified ligand in this calculation may contribute to the lengthening of the Ru−Ru bond length.[35]

The time-dependent DFT (TDDFT) method has been successfully employed in interpreting the spectroscopic properties of $Ru_2(DMBA)_4(CCR)_2$- and $Ru_2(O_2CR)_4Cl$-type compounds.[35,44] As shown in Tables 3 and 4 and Figures 5 and 6, the TDDFT results of **Model1** and **Model2** provide qualitative interpretation of the spectral features for compounds $Ru_2(ap)_4(C{\equiv}CR)$ and $Ru_2(ap)_4(C{\equiv}CR)_2$, respectively. Two sets of allowed transitions were revealed for **Model1**. The first at 692 nm corresponds to the peak observed at 755 nm for compounds **2** and **4** and is attributed to the excitations to

(35) Xu, G.-L.; Crutchley, R. J.; DeRosa, M. C.; Pan, Q.-J.; Zhang, H.-X.; Wang, X.; Ren, T. *J. Am. Chem. Soc.* **2005**, *127*, 13354.
(36) Novozhilova, I. V.; Volkov, A. V.; Coppens, P. *J. Am. Chem. Soc.* **2003**, *125*, 1079.
(37) Stoyanov, S. R.; Villegas, J. M.; Rillema, D. P. *J. Phys. Chem. B* **2004**, *108*, 12175.
(38) Bencini, A.; Ciofini, I.; Daul, C. A.; Ferretti, A. *J. Am. Chem. Soc.* **1999**, *121*, 11418.
(39) Liu, I. P.-C.; Bénard, M.; Hasanov, H.; Chen, I.-W. P.; Tseng, W.-H.; Fu, M.-D.; Rohmer, M.-M.; Chen, C.-h.; Lee, G.-H.; Peng, S.-M. *Chem. Eur. J.* **2007**, *13*, 8667.
(40) Cotton, F. A.; Feng, X. J. *J. Am. Chem. Soc.* **1997**, *119*, 7514.
(41) Bear, J. L.; Han, B.; Huang, S.; Kadish, K. M. *Inorg. Chem.* **1996**, *35*, 3012.
(42) Lin, C.; Ren, T.; Valente, E. J.; Zubkowski, J. D. *J. Chem. Soc., Dalton Trans.* **1998**, 571.
(43) Xu, G.-L.; Campana, C.; Ren, T. *Inorg. Chem.* **2002**, *41*, 3521.
(44) Castro, M. A.; Roitberg, A. E.; Cukiernik, F. D. *Inorg. Chem.* **2008**, *47*, 4682.

Table 3. Band Assignments and TDDFT Predictions for **Model1**

λ (nm)	f	assignment	obs
691.8	0.0754	RuL → δ*	755
		π(Ru−Ru) → δ*	
505.8	0.0467	π(C≡C) → δ*	477
		RuN → π*	
		π(Ru−Ru) → δ*	
		RuL → δ*	
493.8	0.0188	12 transitions	

Table 4. Band Assignments and TDDFT Predictions for **Model2**

λ (nm)	f	assignment	obs
858.7	0.0358	πL → δ*	1050
		πL → σ	
		π → δ*	
758.9	0.0308	πL → σ	
		π → δ*	
		π → σ	
		πL → δ*	
646.1	0.0301	δ → δ*	650
		L → σ	
		RuL → δ*	
574.1	0.1071	π → δ*	
		π → σ	
		πL → δ*	
521.8	0.0699	π → σ	
		π → δ*	
		πL → σ	

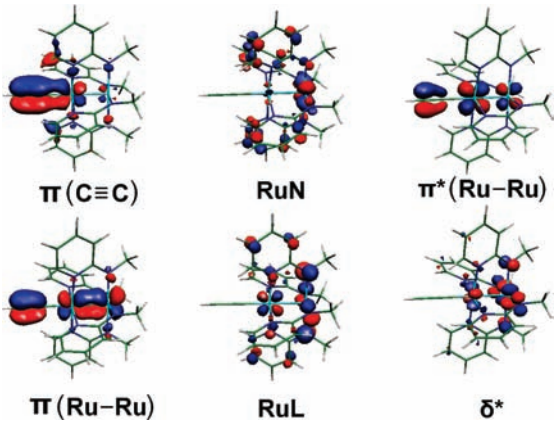

Figure 5. Contour plots of molecular orbitals relevant to band assignments of **Model1**.

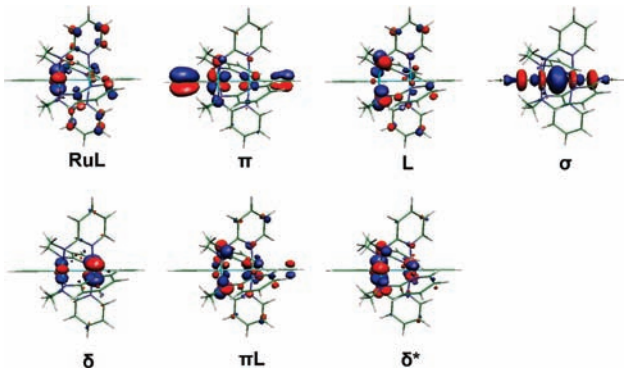

Figure 6. Contour plots of molecular orbitals relevant to band assignments of **Model2**.

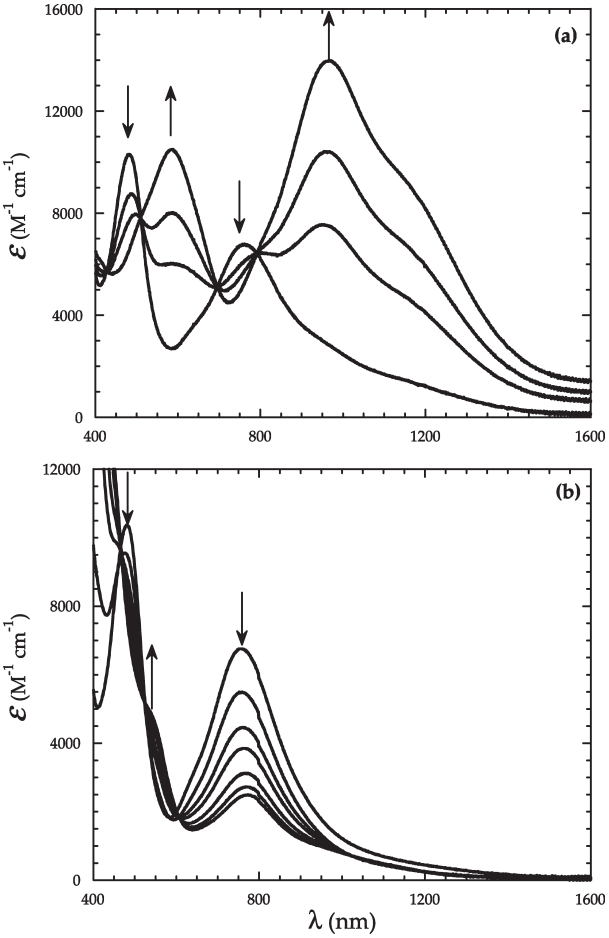

Figure 7. Spectroelectrochemistry of compound **2** upon (a) one-electron oxidation and (b) one-electron reduction.

the δ*(Ru−Ru) orbital from both the RuL and π(Ru−Ru) orbitals. The second transition originates from a group of possible excitations ranging from 494 to 506 nm and corresponds to the intense peak observed at 477 nm. The most prominent contributions come from the excitations to the δ* orbital from both the π(C≡C) and RuN orbitals.

The absorption spectrum of **Model2** was similarly analyzed based on TDDFT calculations (Table 4). The absorption at 1050 nm was calculated at 859 and 759 nm from πL → δ*, πL → σ, π → δ*, and π → σ transitions. The πL → δ*, πL → σ, and π → δ* transitions are assigned as partial ligand-to-metal charge-transfer (LMCT) bands. Furthermore, the band at 650 nm is composed of three sets of calculated absorptions (646, 574, and 522 nm) that consist of several transitions from δ, L, RuL, π, and πL orbitals to δ* and σ orbitals. The π → δ* transition appears at 1050 nm and δ → δ* at 650 nm agrees with the result of our previous spectral assignment for the Ru_2^{6+} analogue.

Spectroelectrochemistry. Studies were performed on solutions of **2** and **3** in 0.20 M Bu_4NPF_6·THF, and the spectral changes are shown in Figures 7 and 8, respectively. Upon one-electron oxidation of **2** (Figure 7a), both peaks were displaced by peaks of equal or higher intensity at longer wavelengths (585 and 966 nm). According to Figure 3, the δ*(Ru−Ru) electron was removed by one-electron oxidation. Consequently, pairing energy is

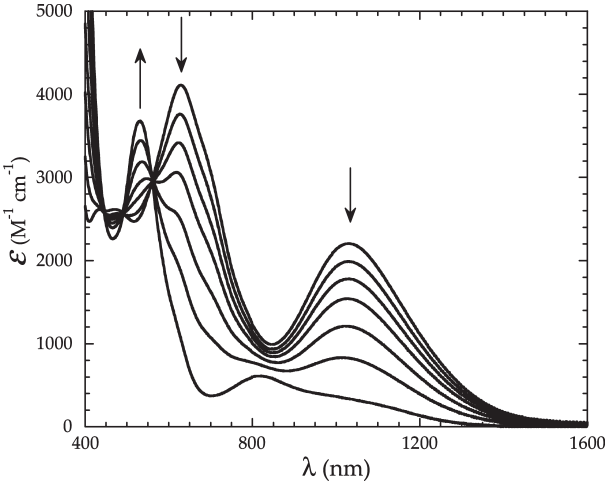

Figure 8. Spectroelectrochemistry of compound **3** upon one-electron reduction.

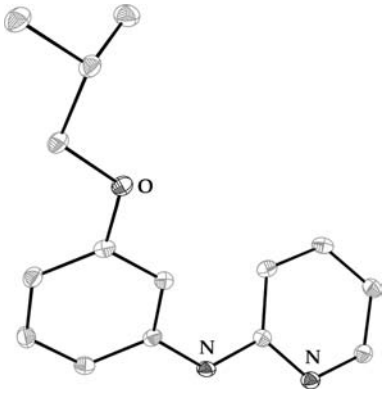

Figure 9. ORTEP plot of H^{i}BuOap.

absent for the excitations to the δ^* orbital of the oxidized species, and both absorptions are shifted to significantly lower energies (longer wavelengths).

Upon one-electron reduction (Figure 7b), the most obvious change is a decrease in the intensity of the $\pi \rightarrow \delta^*$ band at 755 nm. For the energy of this transition to remain essentially unchanged upon the addition of an electron to a π^*(Ru−Ru) orbital suggests that the relative energies of the orbitals in Figure 3 remain unchanged upon reduction. The loss in intensity of this transition is probably due to a reduced contribution to this band from LMCT $\pi_{nb}(N) \rightarrow \delta^*$ transitions (Table 3). The LMCT oscillator strength is dependent upon metal−ligand coupling, which is expected to decrease upon metal-centered reduction.[45]

The spectroelectrochemical oxidation of **3** appears to irreversibly generate oxidized **2**, which upon reduction gave the spectrum of **2** (see the Supporting Information). The spectroelectrochemical reduction of **3** in Figure 8 shows that the addition of an electron to the δ^*(Ru−Ru) orbital shifts transitions to this orbital to higher energies and reduces the intensities of both absorptions. The addition of an electron to δ^* in Figure 4 will result in pairing energy for transitions to this orbital. The loss in intensity must again be attributed to a weakening of the LMCT contributions (Table 4) due to a decrease in metal−ligand coupling with metal-centered reduction.

The one-electron-oxidized **2** and neutral **3** are both $Ru_2^{III,III}$ species, and their visible−NIR electronic absorption bands have similar energies and assignments (compare oxidized **2** in Figure 7 to the spectrum of neutral **3** in Figure 8). However, the extinction coefficients of the bands for oxidized **2** in Figure 7 are considerably greater than those of neutral **3** in Figure 8. This must be related to the presence of the second axial alkynyl ligand in **3**, which would make the Ru centers less electronegative and reduce metal−ligand bonding. As mentioned above, the charge-transfer oscillator strength can be directly related to metal−ligand coupling elements, and so for **3** charge-transfer contributions to these bands are diminished (Table 4). The same arguments can be made for the $Ru_2^{III,II}$ case (Table 3) when reduced **3** (Figure 8) and neutral **2** (Figure 7) are compared.

Conclusion

A new family of $Ru_2(ap)_4$-type compounds with significantly improved solubility was introduced, and their physical properties resemble those of the previously studied $Ru_2(ap)_4$ compounds. Theoretical calculations provided in-depth rationales for spectroscopic data and a greater understanding of magnetic and electronic properties for $Ru_2(ap)_4$-based compounds.

Experimental Section

Phenylacetylene, 1-bromo-2-methylpropane, 2-bromopyridine, and (triisopropylsilyl)acetylene were purchased from Acros. Di-*tert*-butyldicarbonate, 3-aminophenol, trifluoroacetic acid, triethylamine, and *n*-BuLi were from Aldrich, and silica gel was from Merck. $Ru_2(OAc)_4Cl$[46] and 3-(*N*-*tert*-butyloxycarbonylamino)phenol[47] were prepared according to the literature. THF was distilled over Na/benzophenone under an N_2 atmosphere prior to use. ^{1}H NMR spectra were recorded on a Varian 300 NMR spectrometer with chemical shifts (δ) referenced to the residual $CHCl_3$. Visible−NIR spectra were obtained in THF with a Jasco V-670 UV−visible−NIR spectrophotometer. Magnetic susceptibility data were obtained at 293 K using either a Johnson Matthey Mark-I magnetic susceptibility balance or the Evans method. Cyclic voltammograms were recorded in a 0.2 M (n-Bu)$_4$NPF$_6$ solution (THF, N_2-degassed) on a CHI620A voltammetric analyzer with a glassy carbon working electrode (diameter = 2 mm), a Pt-wire auxiliary electrode, and a Ag/AgCl reference electrode. The concentration of diruthenium species is always 1.0 mM. The ferrocenium/ferrocene couple was observed at 0.60 V (vs Ag/AgCl) under the experimental conditions.

Preparation of 2-(3-Isobutoxyanilino)pyridine (H^{i}BuOap). A mixture of 3-isobutoxyaniline (6.7 g, 40 mmol; see the Supporting Information), 2-bromopyridine (4.0 mL, 42 mmol), and potassium carbonate (6.9 g, 50 mmol) was stirred at 140−150 °C for 12 h. The solution was neutralized with a NaOH solution and extracted with CH_2Cl_2. The organic layer was washed with brine and dried over Na_2SO_4. After solvent removal, the residue was crystallized from CH_2Cl_2 and hexanes to yield H^{i}BuOap as white crystals (7.2 g, 73%). Data for H^{i}BuOap. ^{1}H NMR: 8.20 (d, 1H, aromatic), 7.54−7.45

(45) Creutz, C.; Newton, M. D.; Sutin, N. *J. Photochem. Photobiol. A* **1994**, *82*, 47.

(46) Stephenson, T. A.; Wilkinson, G. *J. Inorg. Nucl. Chem.* **1966**, *28*, 2285.

(47) Charpiot, B.; Brun, J.; Donze, I.; Naef, R.; Stefani, M.; Mueller, T. *Biol. Med. Chem. Lett.* **1998**, *8*, 2891.

(m, 1H, aromatic), 7.20 (t, 1H, aromatic), 6.83−6.93 (m, 2H, aromatic), 6.56−6.76 (m, 3H, aromatic), 3.72 (d, J = 3.2 Hz, 2H, $OCH_2CH(CH_3)_2$), 2.13−2.03 (m, 1H, $OCH_2CH(CH_3)_2$), 1.05−1.01 (m, 6H, $OCH_2CH(CH_3)_2$). UV−visible: [λ_{max}, nm (ε, M^{-1} cm^{-1})]: 291 (31 000), 265 (31 600).

Crystal Data for H^{i}BuOap. $C_{15}H_{18}N_2O$, FW = 242.31, triclinic, $P\bar{1}$, a = 5.409(1) Å, b = 10.027(3) Å, c = 12.418(3) Å, α = 75.868(3)°, β = 86.406(3)°, γ = 83.215(3)°, V = 648.2(3) Å^3, Z = 2, D_{calcd} = 1.242 g/cm^3. X-ray diffraction data were collected a Bruker SMART APEX2 CCD diffractometer using Mo Kα at 100 K. Of 37 942 reflections measured, 12 202 were unique (R_{int} = 0.108). Least-squares refinement based on 2916 reflections with $I \geq 2\sigma(I)$ and 163 parameters led to convergence with final R1 = 0.040 and wR2 = 0.105.

Preparation of Ru$_2$(^{i}BuOap)$_4$Cl (1). To a 100 mL round-bottomed flask was added $Ru_2(OAc)_4Cl$ (1.0 g, 2.2 mmol), H^{i}BuOap (2.5 g, 10.3 mmol), LiCl in excess, and 60 mL of toluene, and a Soxhlet extraction apparatus with a K_2CO_3-filled glass thimble was mounted atop the flask. The reaction solution was refluxed for 5 days with K_2CO_3 changed daily during the first 3 days. Upon completion of the substitution reaction as indicated by the ceasing of K_2CO_3 neutralization, thin-layer chromatography analysis revealed the presence of a small amount of byproducts that are of the same color as the main product. These byproducts vanished upon prolonged reflux. After solvent removal, the residue was dissolved in CH_2Cl_2 and filtered. The filtrate was dried, and the residue recrystallized from methanol to yield 2.4 g of blue powder (95% based on Ru). Data for **1**: R_f (CH_2Cl_2/hexanes/Et_3N = 10/10/1, v/v/v) = 0.35. Anal. Found (calcd) for $C_{60}H_{68}ClN_8O_4Ru_2$: C, 59.61 (59.86); H, 5.69 (5.65); N, 9.19 (9.31). Visible−NIR [λ_{max}, nm (ε, M^{-1} cm^{-1})]: 780 (8900), 454 (7200), 416 (7200). Electrochemistry (THF): $E_{1/2}$/V, ΔE_p/V, $i_{backward}/i_{forward}$: B, 0.58, 0.06, 0.96; C, −0.77, 0.06, 0.95. Magnetic data (293 K): χ_g, 4.83 × 10^{-6} esu; χ_{mol} (corr), 6.56 × 10^{-3} esu/mol; μ_{eff}, 3.92 μ_B (3.72 μ_B by the Evans method).

Preparation of Ru$_2$(^{i}BuOap)$_4$(CCPh) (2). To a 20 mL THF solution containing 0.11 mL of phenylacetylene (1 mmol) was added 0.40 mL of n-BuLi (2.5 M in hexanes) at −78 °C. The mixture was slowly warmed to room temperature and stirred for another 1 h to yield an off-white suspension. A portion of the suspension (5.0 mL) was transferred to a Schlenk flask containing a THF solution (30 mL) of Ru$_2$(^{i}BuOap)$_4$Cl (0.240 g, 0.20 mmol). The solution color changed from dark green to brown immediately, and the reaction mixture was stirred for 1 h. Removal of the solvents in vacuo yielded a brown residue, which was rinsed with copious amounts of warm methanol and filtered. A brownish-green solid was obtained after drying in a vacuum and identified as the analytically pure **2**. Yield: 0.166 g (65%). Data for **2**: R_f 0.57 (Et_3N/THF/hexanes, 1/1/10, v/v/v). Anal. Found (calcd) for $C_{68}H_{73}N_8O_4Ru_2$: C, 64.62 (64.33); H, 5.86 (5.75); N, 8.97 (8.83). UV−vis [λ_{max}, nm [ε, M^{-1} cm^{-1})]: 757 (6760), 481 (10 600). IR: ν(C≡C)/cm^{-1} 2045 (w). Electrochemistry: $E_{1/2}$/V, ΔE_p/V, $i_{backward}/i_{forward}$: B, 0.45 0.06, 0.97; C, −0.87, 0.07 1.01 Magnetic data (293 K): μ_{eff}, 3.60 μ_B.

Preparation of Other Ru$_2$(^{i}BuOap)$_4$(CCPh)$_2$ (3). To a 20 mL THF solution containing 0.11 mL of phenylacetylene (1 mmol) was added 0.40 mL of n-BuLi (2.5 M in hexanes) at −78 °C. The mixture was slowly warmed to room temperature and stirred for another 1 h to yield an off-white suspension. A portion of the suspension (10 mL) was transferred to a Schlenk flask containing a THF solution (30 mL) of Ru$_2$(^{i}BuOap)$_4$Cl (0.200 g, 0.166 mmol). The solution color changed from dark green to blue immediately, and the reaction mixture was stirred for 1 h. Removal of the solvents in vacuo yielded a brown residue. The residue was purified on a silica column deactivated with 10% Et_3N in hexanes using a linear gradient of eluents (hexanes/ethyl acetate, 10/1−10/2, v/v) to afford compound **3**. Yield: 0.106 g (50%). Data for **3**: R_f 0.43 (Et_3N/THF/hexanes, 1/1/10, v/v/v). Anal. Found (calcd) for $C_{76}H_{78}N_8O_4Ru_2$: C, 66.51 (66.59); H, 5.81 (5.69); N, 8.14 (8.18). ^{1}H NMR: 9.27 (s, 4H, aromatic), 7.41 (m, 4H, aromatic), 7.14−6.87 (m, 8H, aromatic), 6.54−6.19 (m, 16H, aromatic), 3.01 (m, 8H, $OCH_2CH(CH_3)_2$), 1.20 (m, 4H, $OCH_2CH(CH_3)_2$), 0.8 (m, 24H, $OCH_2CH(CH_3)_2$). UV−vis [λ_{max}, nm (ε, M^{-1} cm^{-1})]: 1030 (2180), 630 (4110), 469 (2730), 433 (2750). IR: ν(C≡C)/cm^{-1}: 2093 (w), 2075 (m). Electrochemistry: $E_{1/2}$/V, ΔE_p/V, $i_{backward}/i_{forward}$: A, 0.77 (E_{pa}); B, −0.42, 0.07, 0.94; C, −1.60, 0.07, 0.47.

Preparation of Ru$_2$(^{i}BuOap)$_4$(CCTips) (4). To a 10 mL THF solution containing 0.09 mmol of ^{i}Pr$_3$SiC$_2$H was added 0.04 mL of n-BuLi (2.5 M in hexanes) at −78 °C. The mixture was slowly warmed to room temperature and stirred for another 1 h to yield a light-yellow solution. This solution was transferred to a flask containing Ru$_2$(^{i}BuOap)$_4$Cl (0.070 g, 0.058 mmol) in 50 mL of THF. The solution color changed from dark green to yellow-green gradually, and the reaction mixture was stirred for 1 h. Removal of solvents in vacuo yielded a green residue, which was rinsed with copious amounts of warm methanol and filtered. A dark-green solid was obtained after drying in a vacuum and identified as pure **4**. Yield: 0.068 g (87%). Data for **4**: R_f = 0.67 (Et_3N/THF/hexanes, 1/1/10, v/v/v). Anal. Found (calcd) for $C_{71}H_{89}N_8O_4Ru_2Si$: C, 63.01 (63.17); H, 6.69 (6.60); N, 8.21 (8.30). UV−vis [λ_{max}, nm (ε, M^{-1} cm^{-1})]: 754 (6080), 473 (8730). IR: ν(C≡C)/cm^{-1}: 1993 (m). Electrochemistry: $E_{1/2}$/V, ΔE_p/V, $i_{backward}/i_{forward}$: B, 0.47, 0.07, 0.96; C, −0.87, 0.10, 1.13. Magnetic data (293 K): μ_{eff}, 3.97 μ_B.

Spectroelectrochemistry of 2 and 3. An OTTLE cell was used to perform spectroelectrochemistry at ambient temperatures.[48] The cell had interior dimensions of roughly 1 × 2 cm with a path length of 0.2 mm and was fitted with a Ag/AgCl reference electrode and indium−tin oxide-coated glass for the working and counter electrodes. All of the spectroelectrochemical transformations showed good reversibility (greater than 95% recovery of original complex spectrum).

Computational Methods. All calculations and geometry optimizations reported in this paper were carried out by using DFT methods[49] with two quantum chemical programs, *Gaussian 03*[30] and *ADF 2006.01*.[29] Because of the convenience in assigning electron occupancy, the studies of electronic configurations were carried out using *ADF*. The spectroscopic assignments (TDDFT) were performed with *Gaussian 03* because of the accuracy of B3LYP.

Full geometry optimizations were performed with symmetry constraints of C_4 (*Gaussian 03*) and C_2 (*ADF*). The z axis coincides with the Ru−Ru axis. The spin-unrestricted formalism was used for the open-shell electronic state, and the spin-restricted formalism was used for the closed-shell one.

In order to study the influence of different exchange-correlation functionals, basis sets, and frozen-core approximations on the geometrical parameters, two types of exchange-correlation functionals (B3LYP and BP86) with different atomic basis sets and frozen-core approximations have been used. Calculations using B3LYP have been carried out with *Gaussian 03*. Two sets of atomic basis sets, referred to as GBI and GBII, were used. In GBI, all-electron-valence double-ζ basis sets (D95V) were used to describe C, N, and H atoms. The valence shell of Ru atoms was described at the double-ζ level (LanL2DZ), and the Los Alamos core potential was used to model the 3s, 3p, and 3d cores of Ru atoms. In GBSII, all-electron 6-31G(d,p) basis sets were used to describe C, N, and H atoms, and LanL2DZ was used for Ru atoms.

Calculations using BP86 have been carried out with *ADF 2006.01*. Two sets of atomic basis sets, referred to as ABI and

(48) Krejcik, M.; DanImagek, M.; Hartl, F. *J. Electroanal. Chem.* **1991**, *317*, 179.

(49) Parr, R. G.; Yang, W. *Density Functional Theory of Atoms and Molecules*; Oxford University Press: New York, 1989.

ABII, were used. In ABI, double-ζ quality for H atoms, double-ζ quality with polarization function for C and N atoms, and triple-ζ quality with polarization function for Ru atoms were used. The inner shells were treated within the frozen-core approximation (1s for C and N and 1s3d for Ru). In ABSII, double-ζ quality for H atoms, double-ζ quality with polarization functions for C and N atoms, and triple-ζ quality with polarization function for Ru atoms. The inner shells were treated within the frozen-core approximation (1s for C and N). Within the *ADF* study, the scalar relativistic zero-order regular approximation was used.

On the basis of the optimized structure (GBI), a TDDFT method[4] was performed to calculate the excited state related to absorption spectra of **Model1** and **Model2**. The solvent effect was studied by the polarized continuum model method. THF was used as the solvent.

Acknowledgment. This work was supported in part by both the National Science Foundation (Grant CHE 0715404 to T.R. and Grant CHE 0541766 to J.D.P. for the purchase of an X-ray diffractometer) and the Natural Sciences and Engineering Research Council of Canada (Grant NSERC to R.J.C.).

Supporting Information Available: Synthesis of the precursors of H^{t}BuOap, spectroelectrochemistry of oxidized **3**, and X-ray crystallographic file in CIF format for H^{t}BuOap. This material is available free of charge via the Internet at http://pubs.acs.org.